Supplementary materials of

Unlocking Dual-Mode Thermal Regulation and Electromagnetic Protection Strategy in Extreme Conditions via Bidirectional Janus Design

Fuhao Yu[1], Pengfei Jia[1], Bibo Wang[1,*], Lei Song[1], Yuan Hu[1]

[1]State Key Laboratory of Fire Science, University of Science and Technology of China, 96 Jinzhai Road, Hefei, Anhui 230026, People's Republic of China.

[*]Corresponding author.

Supplementary materials containing:

*Corresponding author. Fax/Tel: +86-551-63607643
E-mail address: wbibo@ustc.edu.cn (Bibo Wang)

1 Supplementary Experimental Section

1.1 Raw materials

Glycerol, silver nitrate ($AgNO_3$), polyvinyl pyrrolidone (PVP, Mw = 40,000), sodium chloride (NaCl), copper chloride dihydrate ($CuCl_2•2H_2O$, 99 %), and citric acid monohydrate ($C_6H_8O_7•H_2O$) were supplied from Sinopharm Chemical Reagent Co., Ltd. Anhydrous sodium thiosulfate ($Na_2S_2O_3$, 99 %) were purchased from Aladdin Reagent Co. Ltd., China., China. Kevlar fabric (1000d) was supplied by Dingyuan Materials Co., Ltd. Potassium hydroxide (KOH) and dimethyl sulfoxide (DMSO) were purchased from Tianjin Fuyu Chemical Reagent Co., Ltd. (China). Distilled water was made by ourselves and all materials were used without further purification.

1.2 Preparation of AgNWs

Highly uniform AgNWs were synthesized via a modified polyol method based on the reduction of $AgNO_3$ by glycerol in the presence of PVP. Typically, PVP (5.86 g) was dissolved in glycerol (190 mL) at 90 °C with gentle stirring. Next, $AgNO_3$ powder (1.58 g) was added until the solution cooled to 50 °C. Then, a solution containing glycerol (10 mL), NaCl (59 mg), and distilled (DI) water (0.5 mL) was poured into the flask with continuous stirring and heated up to 210 °C. The reaction was stopped after the mixture turned gray-green, and it was poured into beakers. DI water (200 mL) was poured into the solution after cooling to room temperature. Finally, the mixture was purified by centrifuging thrice (8000 rpm, 5 min) with DI water and ethanol. The final AgNWs dispersion (1.2 mg/mL) was suspended in methanol for further use.

1.3 Preparation of Aramid nanofibers (ANF) dispersion

2 g of chopped Kevlar fibers and 1.5 g of KOH were put into 500 mL of DMSO, stirred at ambient temperature for one week, and then the deep-dark-reddish solution was obtained, resulting from the dissociation of hydrogen bonds in Kevlar. Then, 2000 mL of deionized water was added and mechanically stirred for 6 h at 200 rpm to make flocculent ANF fully precipitated. Afterward, ANF was washed with deionized

water for several times in the Brinell funnel until the filtrate was neutral. After being washed, ANF sludge was added with deionized water to 1000 mL and treated with homogenizer at 10000 rpm for 10 min to obtain stable ANF dispersion. The final ANF dispersion (1.2 mg/mL) was suspended in deionized water for further use.

1.4 Preparation of CuS dispersion

Typically, 0.1 M $CuCl_2 \cdot 2H_2O$ and 100 mL deionized water were added to a three-neck flask, and then 10 g polyvinylpyrrolidone (PVP) dissolved in 50 mL deionized water was added into the above solution. After that, 0.1 M 50 mL $Na_2S_2O_3$ solution dripped in the above solution slowly. The pH of the solution was adjusted to 3 using 1 M citric acid, and shaken at 95 °C for 3 h. The final CuS nanosheet dispersion (1.2 mg/mL) was suspended in deionized water for further use.

1.5 Preparation of ACuAg film

The ANF (1.2 mg/mL) and AgNWs (1.2 mg/mL) dispersion was obtained by previous literature. First, 20 mL ANF and a certain amount of CuS dispersion were homogeneously mixed after 1 h at ambient temperature. Then the dark mixed dispersion was filtered through a Celgard membrane (pore diameter: 0.22 μm). Next, the bidirectional Janus film was fabricated by filtering a certain amount of AgNWs dispersion through the ACu network under vacuum. And the content is designed to regulate the conductive network and efficient active/passive radiation heating performance. Then, the ACuAg film was naturally shed from the Celgard membrane by being completely dried at 60 °C.

1.6 Characterizations

Scanning electron microscopy (SEM) images were recorded on a PHILIPS XL30E scanning electron microscope at an acceleration voltage of 5 kV.

X-ray diffraction (XRD) patterns were obtained by a Japan Rigaku Dmax X-ray diffractometer equipped with graphite monochromatized high-intensity Cu K_α radiation (λ= 1.54178 Å).

Fourier transformed infrared (FTIR) analysis was performed on a Nicolet 6700 spectrophotometer (Nicolet Instrument Co., USA), 400 - 4000 cm^{-1}.

X-ray photoelectron spectroscopy (XPS) test was performed with a VG ESCALAB MK-II electron spectrometer (V.G.Scientific Ltd., UK) to investigate the composition of the multifunctional fabrics. The excitation source was an Al K_α ray at 1486.6 eV.

UV-vis-NIR absorption spectrophotometer (Solid 3700, Shimadzu Co., Japan) was used to test the light absorption of multifunctional fabrics, 400 - 2500 nm.

The IR reflectivity (r) and transmittance (τ) were measured using a FTIR spectrometer (Spotlight 200i, PerkinElmer) accompanied by an infrared integrating sphere. The IR emissivity (ε) was then calculated using equation $\varepsilon = 1 - \tau - r$.

The electromagnetic interference shielding properties of the multifunctional fabric were evaluated from those parameters including S11, S22, S12, and S21, which were tested with a vector network analyzer (AV3672, China electronics technology instruments Co., Ltd.) in the 8.2−12.4 GHz region (X-band).

When the electromagnetic wave occurs on a shielding material, the sum of the reflection (R) coefficient, absorption (A) coefficient and transmission coefficient (T) must be 1. The calculation formula for the three parameters is as follows:

$$R = 10^{(S_{11}/10)} \quad (1)$$

$$T = 10^{(S_{21}/10)} \quad (2)$$

$$A = 1 - R - T \quad (3)$$

The total SE (SE_T) consists of the absorption SE (SE_A), reflection SE (SE_R), and multiple internal reflection SE (SE_M), given by the equation:

$$SE_T = SE_R + SE_A + SE_M \quad (4)$$

$$SE_R = -10\log(1 - R) \quad (5)$$

$$SE_A = -10\log(T/(1 - R)) \quad (6)$$

Especially,the SEM is negligible when SET ≥ 15 dB,and then SE_T can be described as

$$SE_T = SE_R + SE_A = -10\log T = |S_{21}| \quad (7)$$

The electrothermal performance was measured with a DC regulated power supply PS-3005D and a thermocouple device, with 10 × 5 mm^2 specimens. Infrared thermal imager (Fluke Tis55, U.S.A.) and digital temperature probe were employed to detect the infrared thermal images and temperature, respectively.

The active and passive heating performance was carried out indoors, in which a DC power supply was connected to a silicon rubber heating plate (JK-003), and a certain voltage was maintained to keep the temperature of the heating plate around 37 °C. A piece of black insulating tape with an emissivity close to human skin was stuck on the heating plate to simulate human skin. Then, the silicone rubber heating plate was wrapped with films, and a K-type thermocouple was used to measure the skin surface temperature under the films. The device is shown in the Manuscript **Figure 2**a and c.

The photothermal property was measured with simulated daylight (CEL-S3500/350, Beijing Zhongjiao Jinyuan Technology Co., Ltd, China), IR baking lamp (808 nm), physiotherapy lamp, and real sunlight as the irradiation source to irradiate the samples vertically at the different light intensity of irradiation. Infrared thermal imager (Fluke Tis55, U.S.A.) and a digital temperature probe were employed to detect the infrared thermal images and temperature, respectively.

The sensing properties of ACuAg were measured through the change in resistance of the sensor during external strain by using a Tektronix DMM4050 digital precision multimeter.

The ACuAg films is placed in a liquid nitrogen environment for testing the ultra-low temperature resistance. The ACuAg films is stored in a high-temperature environment (80, 100, 160 ℃) for 2 hours using High-temperature aging oven for testing the high temperature resistance (Guangdong Bell Test Equipment Co., Ltd.). 1M HCl, NaOH and NaCl aqueous solution was prepared in the laboratory at first, and then ACuAg films is soaked in the above aqueous solution and H_2O for 4 hours for testing the chemical resistance. The XRD and SEM was used to characterize structure changes of the ACuAg films after experiencing extreme environments. In addition, the EMI performance was recorded after the circular bending test (500, 1000, 2000, 3000, 4000, 5000 cycles) at room temperature.

The antibacterial performance of ACuAg was evaluated by *Escherichia coli* (*E. coli*) and *Staphylococcus aureus* (*S. aureus*). Briefly, the ACuAg films (1 × 1 cm^2) were sterilized by ultraviolet light before testing. Then, they were immersed in 2 mL

of diluted bacteria suspension at a concentration of 2 × 106 CFU mL^{-1} and coincubated for 30 min in a shaking incubator. After that, the ACuAg films were added to 10 mL PBS (pH = 7.4) to obtain the bacterial suspension under vigorous oscillation and the obtained suspension samples were diluted 100 times. 100 μL of the diluted bacterial solutions were spread evenly onto fresh Luria-Bertani (LB) agar plates in triplicates and incubated at 37 ℃ for 24 h. The bacterial colonies were photographed and calculated.

2 Supplementary Figures:

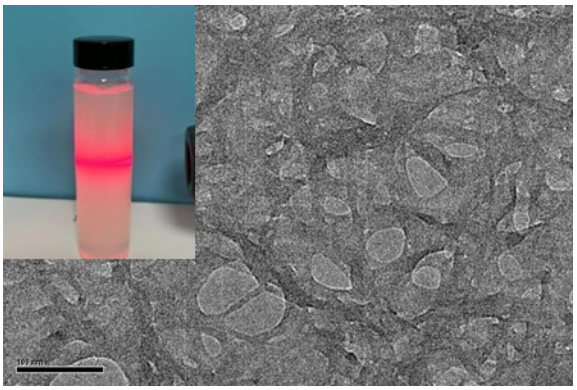

Figure S1. The SEM of ANF.

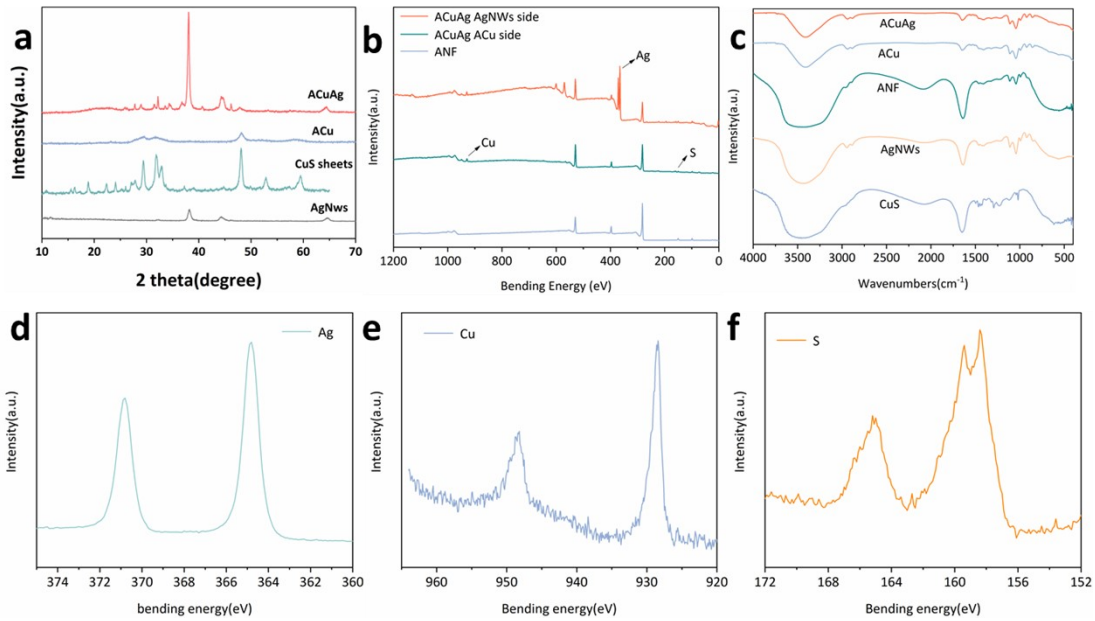

Figure S2. (a) XRD patterns of AgNWs, CuS nanosheets, ACu, and ACuAg films. (b) XPS spectrum of pure ANF, ACu, and ACuAg films. (c) FTIR of AgNWs, CuS nanosheets, prure ANF, ACu, and ACuAg films. (d)Ag 3d, (e) Cu 2p, and (f) S 2p XPS spectrum of the ACuAg film.

The diffraction peaks located around 27.8°, 29.5°, 31.9°, 32.9°, 47.9°, 52.7°, and 59.3° belong to the (101), (102), (103), (106), (110), (108) and (116) crystallographic planes of CuS (**Figure S2a**). The main diffraction peaks of 29.5°, 31.9° and 47.9°appeared in ACu films after the introduction of CuS nanosheets. The four diffraction peaks perfectly match the diffraction peaks (111), (200), (220), and (311)

of face-centered cubic silver (JCPDS No.87-0717). After the ACu surface was filtered into the AgNWs layer, not only all the diffraction peaks of CuS but also the peaks of AgNWs appeared in ACuAg Janus films. In a word, it clearly showed that ACuAg films exhibited the characteristic diffraction peaks of CuS and AgNWs, declaring the successful preparation of bidirectional Janus structure step by step. Besides, the X-ray photoelectron spectroscopy (XPS) test was used to further investigate the surface chemistry of Janus films. As confirmed by XPS wide-scan spectra, the Cu and S signals of ACu films revealed the successful preparation of a high emission layer (**Figure S2b** and **d~f**). Furthermore, the appearance of additional Ag signals compared with ACu films indicates the introduction of the AgNWs layer to construct bidirectional structure (**Figure S2b** and **d**). And the Fourier transform infrared spectroscopy (**Figure S2c**) could also prove the above conclusion.

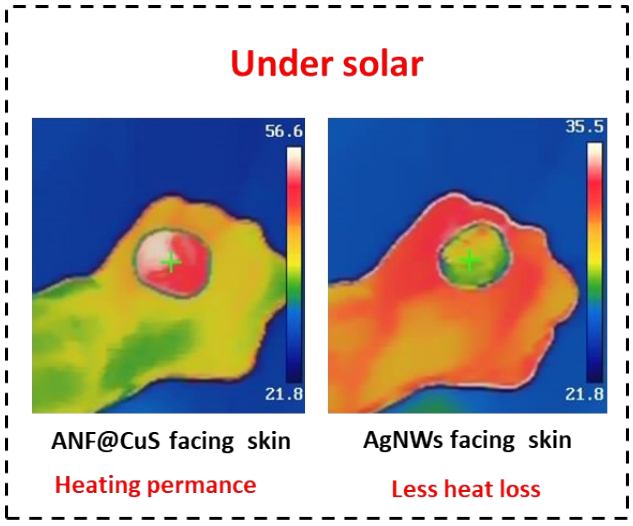

Figure S3. The IR image of ACuAg films covered human skin.

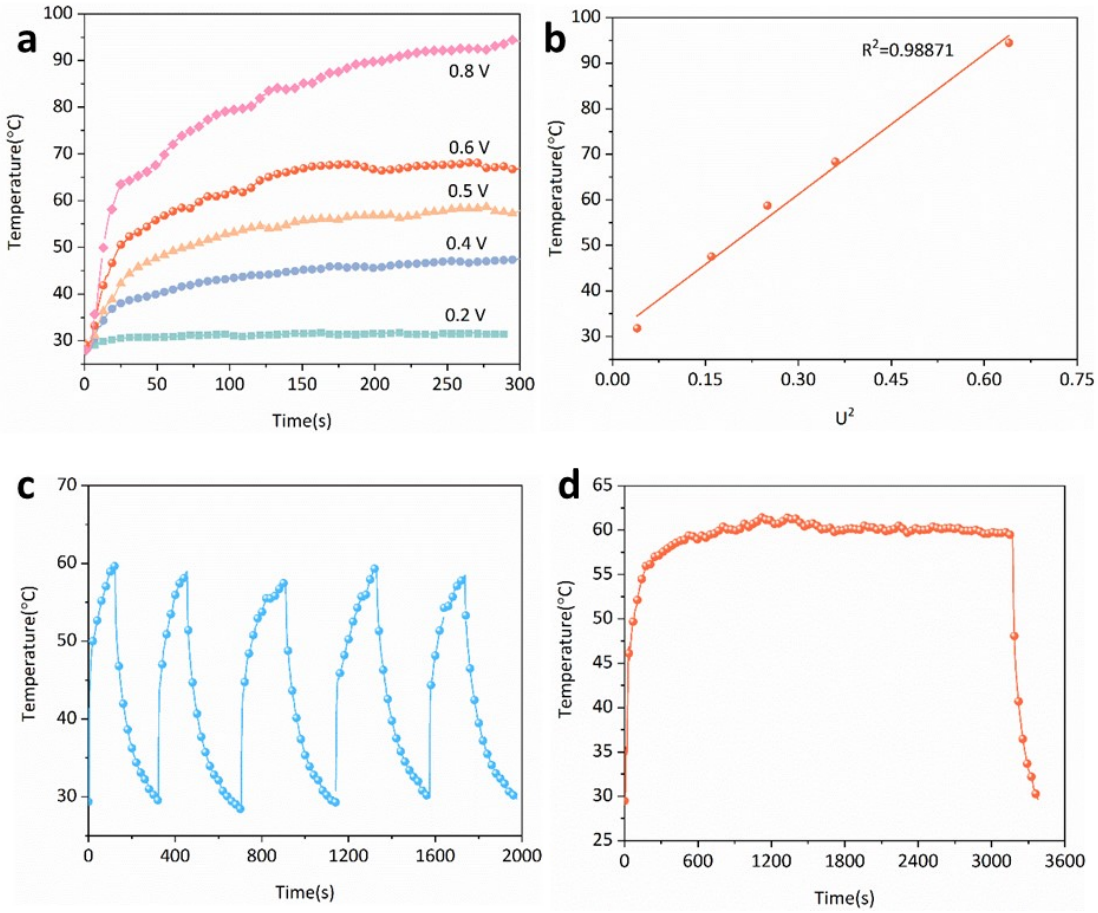

Figure S4. Electrothermal performance. (a) A surface temperature change of ACuAg film with distinct voltages. (b) U^2-T curves of ACuAg at different voltages. (c) Cyclic electrothermal heating and cooling performance of the ACuAg at 0.5 V. (d) Temperature stability for a long time using PDMS@CuS@PSF under a driving voltage of 0.5 V standing.

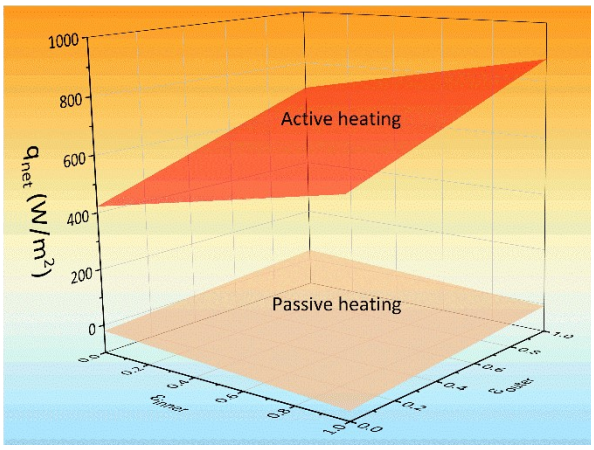

Figure S5. The net heat flux q_{net} of film with the change of inner surface emissivity (ε_{in}) and outer surface emissivity (ε_{out}).

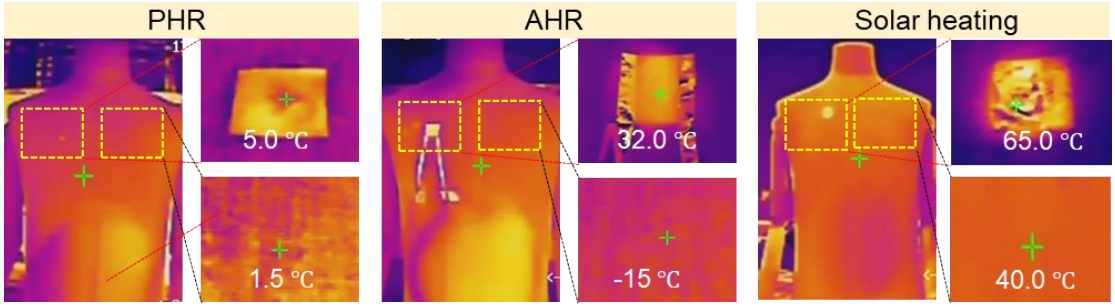

Figure S6. The PHR, AHR and solar heating performance under real realistic scenarios. Use a low-temperature oven (Guangdong Bell Test Equipment Co., Ltd.) to create a low-temperature environment. The PHR and AHR was tested under 2 ℃ and -20 ℃. The solar heating performance was tested under real sunlight (11:00 AM, Hefei, Anhui province, China)

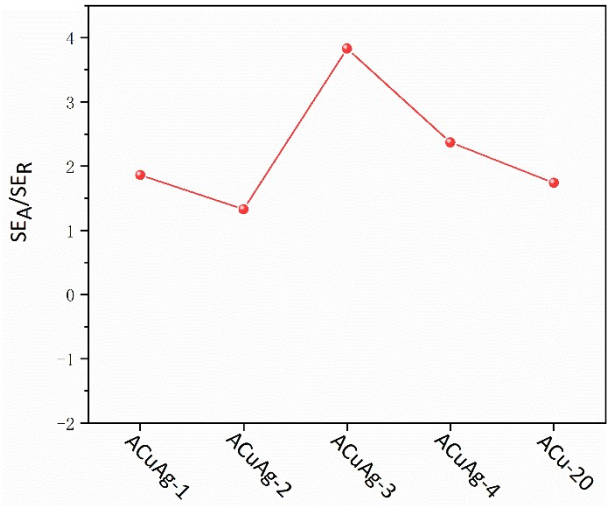

Figure S7. SE_A/SE_R of different films

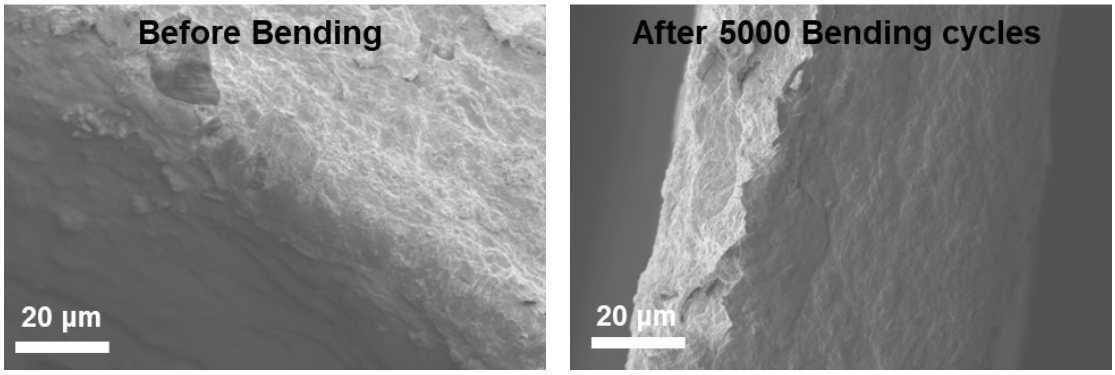

Figure S8. The SEM of ACuAg films before and after bending test

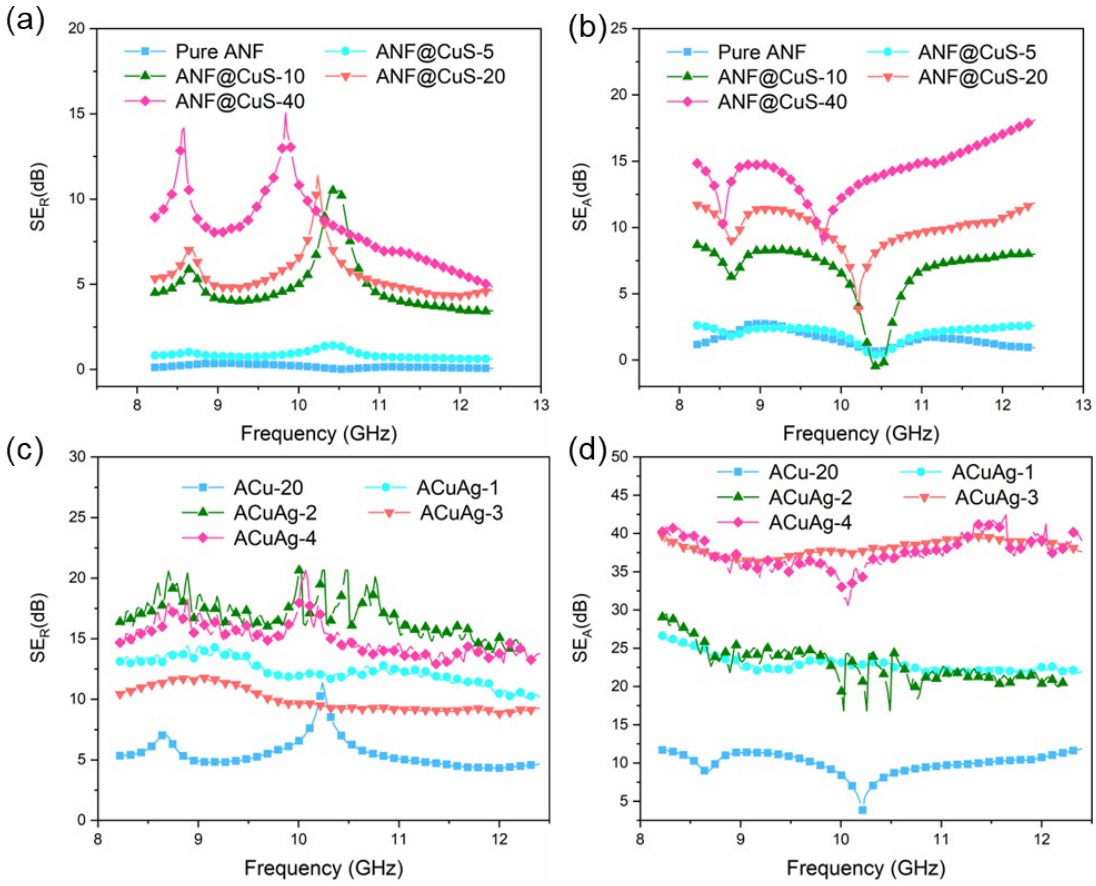

Figure S9. The (a) SE_R and (b) SE_A of ACu films with different CuS contents. The (c) SE_R and (d) SE_A of ACuAg films with different AgNWs contents.

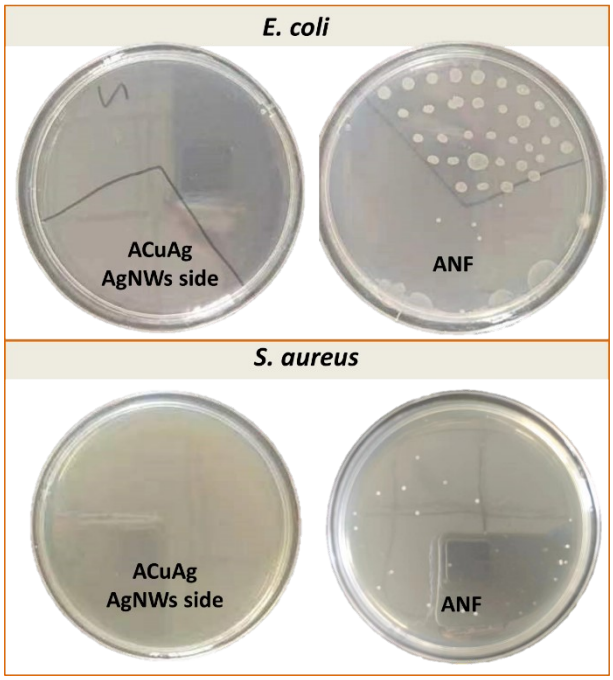

Figure S10. Antibacterial property of ACuAg films

3 Supplementary Notes

Supplementary Notes S1: Calculation of average mid-IR spectral emissivity

The average mid-IR spectral emissivity at 7~14 μm of ACuAg film was calculated according to the following equations [1, 2]:

$$\varepsilon_T(T) = \frac{\int_7^{14} \varepsilon_\lambda(\lambda,T)L(\lambda,T)d\lambda}{\int_7^{14} L(\lambda,T)d\lambda}$$

$$L(\lambda,T) = \frac{C_{1L}}{\lambda^5[\exp\left(\frac{c_2}{\lambda T}\right) - 1]}$$

where $\varepsilon_\lambda(\lambda, T)$ is the spectral emissivity measured based on the thermal radiation relation, $\varepsilon = 1 - r - \tau$ (ε, r and τ are emissivity, reflectivity and transmissivity, respectively). The r and τ were obtained from a FTIR spectrometer (Spotlight 200i, PerkinElmer) accompanied by an infrared integrating sphere. λ is the spectral radiance emitted from the blackbody, in which C_{1L} is the first radiation constant for spectral radiance, $C_{1L} = 2hc^2 = 1.191 \times 10^8$ (W.μm^4. m^{-2}.sr). C_2 is the second radiation constant, $C_2 = hc/K_B = 1.439 \times 10^4$ (μm.K). K_B is the Boltzmann constant, h is the

Planck constant, and *c* is the speed of light in a vacuum. *T(K)* is the room temperature (298 K) when measuring the spectral emissivity.

Supplementary Note S2: Heat transfer analysis for indoor radiative heating:

The heat transfer analysis for indoor radiation heating is based on the one-dimensional steady-state heat transfer model [3-5]. The room temperature is assumed to be 20°C and the skin temperature is maintained at 37°C. For passitive radiation heating modes, the net heat flux (q_{net}) can be composed of:

Passive radiation heating analysis

Heat balance at skin surface:

$$q_{net} = q_{gen} = q_{rad,Ag} - (1 - r_{Ag}) \cdot q_{rad,s} - q_{cond,a}$$

Heat balance at film outer surface:

$$q_{net} = q_{gen} = (1 - r_{ACu}) \cdot q_{rad,e} - q_{rad,ACu} - q_{conv}$$

Active radiation heating analysis

Heat balance at skin surface:

$$q_{net} = q_{gen} = q_{rad,Ag} - (1 - r_{Ag}) \cdot q_{rad,s} - q_{cond,a}$$

Heat balance at film outer surface:

$$q_{net} = q_{gen} = (1 - r_{ACu}) \cdot q_{rad,e} - q_{rad,ACu} - q_{conv} + q_{Joule}$$

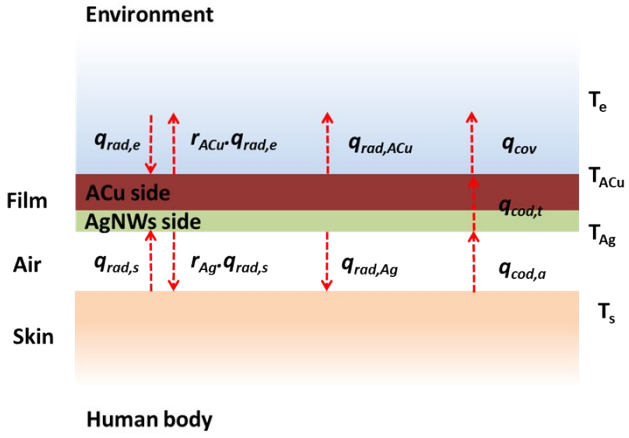

Figure S11. One-dimensional steady-state heat transfer model of PHR.

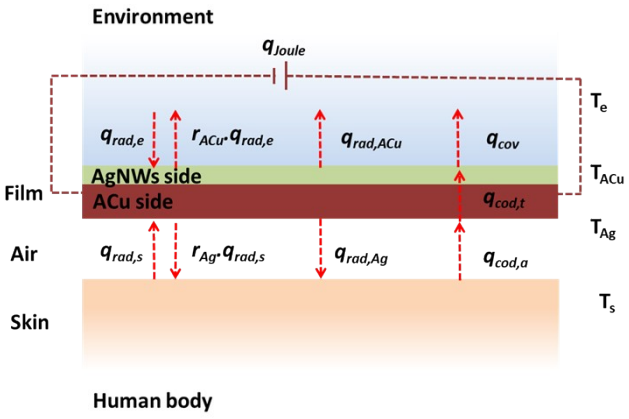

Figure S12. One-dimensional steady-state heat transfer model of AHR.

$q_{rad,Ag}$: the radiative heat flux from the AgNWs layer;

$q_{rad,ACu}$: the radiative heat flux from the ACu layer;

$q_{rad,e}$: the radiative heat flux from the indoor environment;

$q_{rad,s}$: the radiative heat flux from the skin;

$q_{con,\ a}$: the conduction heat flux from the air gap between the skin and the ACuAg films;

q_{cond}: the convective heat flux from the textile to the environment.

4 Supplementary tables

Table S1. The relevant parameters used during different steps.

	ANF dispersion (mL)	CuS dispersion (mL)	AgNWs dispersion (mL)	Thickness (μm)
ACu-5	10	2.5		7
ACu-10	10	5		12
ACu-20	10	10		13
ACu-40	10	20		13
ACuAg-1	10	10	2.5	12
ACuAg-2	10	10	5	12
ACuAg-3	10	10	7.5	12
ACuAg-4	10	10	10	12

Table S2. Comparison of Mid-infrared characteristics of different film materials

Materials	Emissivity	Reflectivity	Strength (MPa)	Ref.
Ag	0.064	0.936	134.2	
Cu	0.106	0.894	204.8	
Al	0.093	0.907	112	
Graphene	0.353	0.647	177.2	
MWNTs	0.16	0.84	150.9	
MXene	0.09	0.91	44.8	
MWNTs/CA fabrics	0.90	0.10	/	[6]
CB coatings	0.96	0.04	/	[7]
PE/MXene	0.96	0.89		[8]
PVDF-HFP/ZrO @Mxene/CNT	0.93	0.07	/	[9]
ACuAg films	0.89	0.90	196	This work

Table S3. Comparison of electrothermal and photothermal conversion of different materials.

Materials	Electrothermal		Photothermal		Ref.
	DC (V)	Temperature (℃)	Irradiation (kW/m^2)	Temperature (℃)	
MWNTs/EP	25	89.5	1.5	45.4	[10]
CF/TiO2/PPy	3	130	1	65	[11]
Ni-P/NWs	5	133.5	0.85	77.9	[12]
CNS/AMS	1	48	2	92	[13]
Ta4C3TX/GAs	1	42.2	1	90.2	[14]
BC@Fe_3O_4/CNT/$Ti_3C_2T_x$	1	35.6	1	101.5	[15]
MXene-Coated fabic	5	76	1.25	107	[16]
MXene/cellulose	2.5	83.8	1	116	[17]
CNTs@MXene	4	105	1	50	[18]
ACuAg films	0.8	95	1	75	This work

Table S4 SE_T versus thickness of ACuAg films compared with previously reports based on films.

Samples	**Thickness (μm)**	**EMI (dB)**	**Ref**
MXene/ANF films	93	38	[19]
MXene/ANF films	13	43	[20]
PE@PET/MXene films	143	50.4	[21]
BC@MXene@AgNWs	100	47	[22]
PI/PEDOT: PSS/MWNTs	47	32.69	[23]
MXene-BP-MXene(Ni)	60	51.2	[24]
PI@MXene	900	54.5	[25]

Polyimide Fiber@MXene	260	49.9	[26]
MXene/CNF/CNT	380	38.4	[27]
PDMS/LM	150	44.7	[28]
LM/CNT/PDMS	2000	42.6	[29]
rGO/PVA	360	20.3	[30]
CF/PC	292	38.6	[31]
This Work	**12**	**53**	**This work**

Reference:

[1] T. Echániz, I. S. Fernández, R. Pérez-Sáez, C. Prieto, R. Escobar Galindo, M. Tello, Sol. Energy Mater. Sol. Cells 2015, 140, 249-252.

[2] P. Wang, Z. Hu, Z. Xie, M. Yan, Rev. Sci. Instrum. 2018, 89, 054903.

[3] M. Shi, M. Shen, X. Guo, X. Jin, Y. Cao, Y. Yang, W. Wang, J. Wang, ACS Nano 2021, 15, 11396-11405.

[4] L. Cai, A. Song, P. Wu, P. Hsu, Y. Peng, J. Chen, C. Liu, P. Catrysse, Y. Liu, A. Yang, C. Zhou, C. Zhou, S. Fan, Y. Cui, Nat. Commun. 2017, 8, 496.

[5] H. Luo, Q. Li, K. Du, Z. Xu, H. Zhu, D. Liu, L. Cai, P. Ghosh, M. Qiu, Nano Energy 2019, 65, 103998.

[6] C. Mo, X. Lei, X. Tang, M. Wang, E. Kang, L. Xu, K. Zhang, Nanoengineering Natural Leather for Dynamic Thermal Management and Electromagnetic Interference Shielding, Small 2023, 19, 2303368.

[7] P. Cui, Y. Yan, H. Wei, S. Wu, S. Zhong, W. Sun, Study of Manipulative Pore Formation upon Polymeric Coating for the Endowment of the Switchable Property between Passive Daytime Radiative Cooling and Heating, ACS Appl. Mater. Interfaces 2024, 16, 33, 44044–44054.

[8] M. Shi, Z. Song, J. Ni, X. Du, Y. Cao, Y. Yang, W. Wang, J. Wang, Dual-Mode Porous Polymeric Films with Coral-like Hierarchical Structure for All-Day Radiative Cooling and Heating, ACS Nano 2023, 17, 3, 2029–2038.

[9] X. Meng, Q. Zhao, Z. Chen, Q. Li, X. Chen, A Janus film coupling radiative cooling and heating for all-day active/passive personal thermal management, Materials Today Physics 46 (2024) 101511.

[10] Y. Guo, H. Zhao, C. Zhang, G. Zhao, Super photothermal/ electrothermal response and anti-icing/deicing capability of superhydrophobic multi-walled carbon nanotubes/epoxy coating, Chemical Engineering Journal 497 (2024) 154383.

[11] X. Li, Y. Chen, B. Zhu, M. Salimi, L. Zhang, M. Amidpour, M. Zhu, Z. Chen, Biomimetic Design of Photothermal/Electrothermal Fabric Composed of Carbon-Core/Nanorod-Array-Shell Fibers for Efficient All-Weather Seawater

Evaporation, Adv. Funct. Mater. 2025, 2423472.

[12] E. Khajeh, K. Nasouri, G. Askari, M. Mandegari, Flexible and lightweight metalized polyamide nonwoven for electromagnetic interference shielding, electrothermal, photothermal, and antibacterial applications, Chemical Engineering Journal 502 (2024) 158203.

[13] Z. Li, Z. Lin, M. Han, Y. Mu, P. Yu, Y. Zhang, J. Yu, Flexible electrospun carbon nanofibers/silicone composite films for electromagnetic interference shielding, electrothermal and photothermal applications, Chemical Engineering Journal 420 (2021) 129826.

[14] Z. Li, J. Zhang, Y. Zhao, F. Wu, T. Lv, L. Yu, C. Yu, C. Zhao, G. Xing, $Ta_4C_3T_X$ /graphene aerogels with combined photo/electro-thermal conversion performa nces for multifunctional applications, ChemicalEngineeringJournal489(2024)1 51196.

[15] Y. Yang, L. Shao, J. Wang, Z. Ji, T. Zhang, M. Wu, Y. He, C. Wang, J. Ma, An As ymmetric Layer Structure Enables Robust Multifunctional Wearable Bacteria l Cellulose Composite Film with Excellent Electrothermal/Photothermal and EMI Shielding Performance, Small 2024, 20, 2308514.

[16] X. Wang, Z. Lei, X. Ma, G. He, T. Xu, J. Tan, L. Wang, X. Zhang, L. Qu, X. Zha ng, A lightweight MXene-Coated nonwoven fabric with excellent flame Ret ardancy, EMI Shielding, and Electrothermal/Photothermal conversion for we arable heater, Chemical Engineering Journal 430 (2022) 132605.

[17] Z. Guo, Y. Zhao, P. Luo, J. Wang, L. Pei, H. Yu, P. Song, F. Ren, P. Ren, Asym metric and mechanically enhanced MOF derived magnetic carbon-MXene/ce llulose nanofiber films for electromagnetic interference shielding and electro thermal/photothermal conversion, Chemical Engineering Journal 497 (2024) 155707.

[18] Y. Zhang, W. Wang, J. Xie, K. Dai, F. Zhang, Q. Zheng, Smart and flexible C NTs@MXene heterostructure-decorated cellulose films with excellent electrot hermal/photothermal conversion and EMI shielding performances, Carbon 20 0 (2022) 491–499.

[19] M. Ma, W. Shao, Q. Chu, W. Tao, S. Chen, H. He, Y. Zhu, X. Wang, J. Mater. Chem. A 2024, 12, 1617-1628.

[20] C. Li, L. Qi, J. Fei, J. Yan, Z. Wu, T. Zhang, H. Li, Carbon 2024, 217, 118620.

[21] Z. Sha, H. He, H. Ma, B. Hong, J. Lu, X. Fei, M. Zhu, Carbon 2024, 216, 118595.

[22] Y. Zhang, G. Zhang, Z. Ma, J. Qin, X. Shen, Nano Research, ISSN 1998-0124 CN 11-5974/O4.

[23] X. Liu, L. Tian, Z. Bao, Y. Zhang, P. Qian, W. Geng, D. Zhang, Q. Zhu, H. Geng, ACS Appl. Mater. Interfaces 2024, 16, 17, 22391-22402.

[24] C. Wen, B. Zhao, Y. Liu, C. Xu, Y. Wu, Y. Cheng, J. Liu, Y. Liu, Y. Yang, H. Pan, J. Zhang, L. Wu, R. Che, Adv. Funct. Mater. 2023, 2214223.

[25] Y. Cheng, X. Li, Y. Qin, Y. Fang, G. Liu, Z. Wang, J. Matz, P. Dong, J. Shen, M. Ye, Sci. Adv. 2021, 7, 1663.

[26] J. Yao, L. Zhang, F. Yang, Z. Jiao, X. Tao, Z. Yao, Y. Zheng, J. Zhou, Chem. Eng. J. 2022, 446, 136945.

[27] W. Cao, C. Ma, S. Tan, M. Ma, P. Wan, F. Chen, Nano-Micro Lett. 2019, 11, 1-17.

[28] G. Wang, J. Chen, W. Zheng, B. Shen, Chem. Eng. J. 488 (2024) 151052.

[29] Y. Wang, Y. Gao, T. Yue, X. Chen, M. Wang, Applied Surface Science 563 (2021) 150255.

[30] B. Yuan, C. Bao, X. Qian, L. Song, Q. Tai, K. Liew, Y. Hu, Carbon 2014, 75, 178-189.

[31] W. Tang, L. Lu, D. Xing, H. Fang, Q. Liu, K. Teh, Composites Part B: Engineering 2018, 152, 8-16.